Symmetry breaking: A heuristic approach to chaotic scattering in many dimensions

L. Benet,[1,2] J. Broch,[3,2] O. Merlo,[3,2] and T. H. Seligman[1,2]
[1]*Centro de Ciencias Físicas, U.N.A.M., Apartado Postal 48-3, 62251 Cuernavaca, Morelos, México*
[2]*Centro Internacional de Ciencias A.C., Apartado Postal 6-101, 62131 Cuernavaca, Morelos, México*
[3]*Institut für Physik, Universität Basel, Klingelbergstrasse 82, CH-4056 Basel, Switzerland*
(Received 5 October 2004; published 30 March 2005)

As the theory of chaotic scattering in high-dimensional systems is poorly developed, it is very difficult to determine initial conditions for which interesting scattering events, such as long delay times, occur. We propose to use symmetry breaking as a way to gain the insight necessary to determine low-dimensional subspaces of initial conditions in which we can find such events easily. We study numerically the planar scattering off a disk moving on an elliptic Kepler orbit, as a simplified model of the elliptic restricted three-body problem. When the motion of the disk is circular, the system has an integral of motion, the Jacobi integral, which is no longer conserved for nonvanishing eccentricity. In the latter case, the system has an effective five-dimensional phase space and is therefore not amenable for study with the usual methods. Using the symmetric problem as a starting point we define an appropriate two-dimensional subspace of initial conditions by fixing some coordinates. This subspace proves to be useful to define scattering experiments where the rich and nontrivial dynamics of the problem is illustrated. We consider in particular trajectories which take very long before escaping or are trapped by consecutive collisions with the disk.

DOI: 10.1103/PhysRevE.71.036225 PACS number(s): 05.45.Jn, 05.45.Pq

I. INTRODUCTION

The classical dynamics of scattering systems, in particular its chaotic manifestations, is well understood for open Hamiltonian systems with two effective degrees of freedom. Typical examples are one-dimensional periodically kicked driven systems and conservative (time-independent) ones of two degrees of freedom. The effective dimension of phase space is then 3. In such cases the dynamics are determined by the properties of the invariant set or chaotic saddle. Smale's horseshoe construction can then be performed on an appropriate surface of section [1–4] and explains adequately the topology and symbolic dynamics of such a problem.

Unfortunately the situation becomes qualitatively more complex for higher dimensions. Not only is the surface of section no longer two dimensional and thus not easy to draw and understand, but fundamental differences occur; e.g., invariant tori no longer separate the phase space, giving rise to Arnold diffusion, and besides hyperbolic and elliptic fixed points also loxodromic ones can appear. Wiggins and coworkers [5,6] have made some progress in characterizing the invariant manifolds of Hamiltonian flow in higher dimensions, but we are far from a useful understanding of the chaotic saddle in the general situation.

In the present paper we will take a pragmatic approach and attempt to find a two-dimensional subspace of initial conditions for the chaotic scattering process, such that a chart of delay times over this space will yield the relevant information. We shall choose a planar elliptic restricted three-body problem to carry out such an analysis, because this problem is of considerable importance and much discussed in the literature. We shall not use the $1/r$ potential, but a simpler hard-disk model, which conserves the relevant features and is particularly easy to handle [7]. Even in this simpler problem the total space of initial conditions is five-dimensional, so the choice of the subspace requires a considerable physical insight, or plain luck, to an unreasonable degree. We shall thus opt for a particular, but very important situation, where the physical insight is systematically available.

A common route for dimensional reduction of a system is the existence of a continuous symmetry, which leads to a conserved quantity. We can hope therefore that a slight breaking of such a symmetry, while putting us abruptly in a higher-dimensional space, will nevertheless leave an important mark on the system, which will in some sense slowly vanish as symmetry breaking increases. On the other hand, this case is certainly not irrelevant, but rather occurs quite frequently in practice; see, for instance, [8,9]. It would certainly be interesting to search for a group-theoretical interpretation of such a procedure, and some work exists in this respect [10], but this would lead us well beyond the scope of the present analysis.

In our chosen example—namely, the restricted three-body problem—the constant of motion in question is the Jacobi integral [11] which is conserved when the orbits of the two heavy bodies are exactly circular. While this is probably never the case in a real system, small eccentricities of orbits are quite common. In particular we have an interest in narrow planetary rings [12–14] with shepherd moons; they typically have small eccentricities. Such is the case, e.g., for the moons accompanying Saturn's F ring or Uranus' ϵ ring [15].

The paper is organized as follows: In the next section we shall describe the hard-disk model we use and reexamine the circular case. In Sec. III we choose the subspace of initial conditions. In Sec. IV we analyze the charts we obtain for our problem and consider the implications for the dynamics of orbits trapped permanently or at least for very long times. Finally, we draw some conclusions.

II. DESCRIPTION OF THE MODEL

We study the planar scattering of a point particle off a hard-disk on a two-dimensional periodic orbit. The center of the disk moves on an elliptic Kepler orbit with one focus at the origin. The phase space of this system is therefore five dimensional (two and a half degrees of freedom): Two coordinates and two canonically conjugated momenta define the position in phase space of the particle, and one angle (or initial phase) determines the initial position of the disk along the Kepler orbit. As we shall see below, the special case of a circular orbit allows for a reduction of the dimensionality of the problem due to Jacobi's integral of motion.

The Kepler orbit can be parametrized as [16]

$$x = a(\cos E - \varepsilon), \tag{1}$$

$$y = a(1 - \varepsilon^2)^{1/2} \sin E, \tag{2}$$

$$t = (a^3/K)^{1/2}(E - \varepsilon \sin E). \tag{3}$$

Here, a represents the semimajor axis of the ellipse, $\varepsilon \in [0,1)$ is the eccentricity, K is a strength parameter (below set equal to 1), and E is the eccentric anomaly. The foci of the ellipse define the x axis of the fixed coordinate frame (sidereal frame), the periapsis of the ellipse defines the positive x direction, and the motion along the ellipse is counterclockwise. We observe that the Kepler equation [Eq. (3)], which relates the physical time t with E, implies that such an elliptic orbit is a solution of the two-body Kepler problem. An alternative parametrization is the usual one in polar coordinates,

$$r = \frac{a(1 - \varepsilon^2)}{1 + \varepsilon \cos(\phi - \phi_0)}. \tag{4}$$

Here ϕ is the polar angle at time t and ϕ_0 is the initial position of the disk along the Kepler orbit with respect to the periapsis (initial phase). The polar angle ϕ is related to the physical time by $r^2\dot{\phi} = [Ka(1-\varepsilon^2)]^{1/2}$, $\dot{\phi}$ denoting the time derivative of ϕ. In the following, we define the units by $a = 1$ and $K = 1$. In these units, the time t is also called mean anomaly and the orbital period is 2π.

The dynamics of the scattering system are as follows. The particle moves freely until it encounters the disk. No collision leads to open motion; i.e., the particle escapes from the interaction region. If a collision takes place, the particle is specularly reflected with respect to the local (moving) frame, at the collision point. This defines the outgoing conditions after the collision. In general, the result of a collision depends on the position where the collision occurs on the disk, the relative velocities, and for nonvanishing ε, on the position along the elliptic trajectory of the disk.

When the eccentricity is zero, the motion of the disk is uniformly circular and there exists a constant of motion, the Jacobi integral. This quantity corresponds to the Hamiltonian in a rotating (synodic) frame of appropriate constant angular velocity. From the fact that the orbit of the disk is circular, the primitive periodic orbits of the system (in the rotating or synodic frame) can be easily identified with the orbits of consecutive radial collisions [7]. These orbits satisfy the relation

$$v = \frac{\tilde{v}}{\omega(a-d)} = \frac{2\cos\beta}{\pi(2n+1) - 2\beta} = -\frac{2\cos\theta}{\pi(2n-1) + 2\theta}. \tag{5}$$

Here v is the dimensionless magnitude of the velocity vector in the fixed frame ($\tilde{v}$ is the physical velocity and $\omega = 1$ is the rotation frequency), $\beta \in [-\pi/2, \pi/2]$ is the angle formed by the outgoing trajectory with respect to the normal at the collision point, and $\theta = \pi - \beta$, $\pi/2 \leqslant \theta \leqslant 3\pi/2$. The parameter $n = 0,1,2,\ldots$ defines the number of full turns that the disk completes between consecutive collisions. From Eq. (5), an explicit expression for the Jacobi integral as a function of β (or θ) can be derived [7]. Conservation of the Jacobi integral leads naturally to a reduction of the dimensionality of the problem and allows us to use standard methods to study the chaotic saddle [7].

For nonzero eccentricity there is no constant of motion, and Poincaré sections cannot be used easily because in the present case they would be four dimensional. In particular, for nonzero ε there is a nontrivial dependence of the outcome of the collisions with respect to the position ϕ on the orbit of disk. By consequence, the construction of the primitive periodic orbits for the circular problem may not be helpful in the eccentric case. Yet they allow us to prove the existence of periodic orbits in the system for small eccentricities. We must thus rely on an exploration of the structure of the space of initial conditions of this system, e.g., in terms of the number of collisions, for different values of ε. This can be used to define meaningful one-parameter scattering experiments that sample distinct regions of the chaotic saddle in phase space.

III. SPACE OF INITIAL CONDITIONS

A. Definitions

As mentioned above, the space of initial conditions is five dimensional. This space can be characterized by the angle ϕ_0 with $-\pi \leqslant \phi_0 \leqslant \pi$, which denotes the initial position of the center of the disk, and the two coordinates and momenta which specify the initial conditions of the particle. For concreteness, we restrict the initial position of the particle to be on the disk. This allows us to use only the angle $\alpha \in [0, 2\pi]$ to specify completely the initial position of the particle. This choice implicitly selects the scattering events that lead to a collision with the disk at the position characterized by α and ϕ_0. For the initial outgoing velocity of the particle, we still require two quantities; we choose the magnitude of the velocity v and its direction as defined above by the angle θ. Figure 1 illustrates the definition of the set of initial parameters. This space is four dimensional, which is still too large to be explored numerically, in particular in order to consider the regions in phase space where nontrivial dynamics takes place [5,6,17].

We shall further fix the angles ϕ_0 and α, thus leading to an effective two-dimensional space of initial conditions. These two angles can in principle be arbitrarily fixed. We

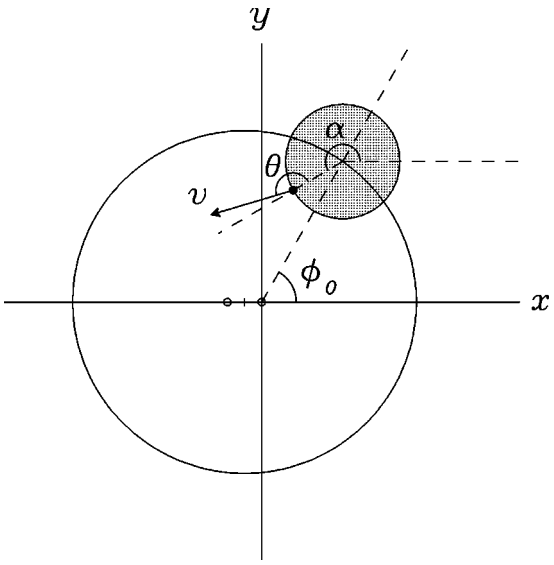

FIG. 1. Definition of the initial conditions for the scattering setup: ϕ_0 denotes the initial position of the center of the disk along the Kepler orbit, α denotes the initial position of the particle on the disk (initial collision point), and v denotes the (scaled) magnitude of the outgoing velocity and θ defines its direction. The foci of the ellipse are shown on the x axis as open circles (○) and the center by a cross (+). The origin of the coordinate system is one focus of the ellipse.

recall that in the circular case the primitive periodic orbits correspond to radial collisions, which is geometrically expressed as $\alpha-\phi_0=\pi$. Intuitively, we expect that for small eccentricity the periodic orbits lie somewhat close to those of the circular case. Guided by the circular case, we shall therefore fix $\alpha-\phi_0=\pi$. Yet the rotational symmetry of the circular case provides no further guide to define another condition which involves these two angles. We arbitrarily consider the condition $\phi_0=0$, unless otherwise explicited (cf. Sec. IV). This situation corresponds to exploring the events which display a collision at the periapsis. If there exists a periodic orbit bouncing at this position or, at least, if the stable or unstable manifolds of an unstable periodic orbit have a component at $\phi_0=0$, our scattering experiments will detect them. Clearly, our analysis can be extended to any values of ϕ_0 and α.

In the numerical results presented below, we fix the radius of the disk to $d/a=1/3$. The numerical value of d/a does influence the stability properties of the trapped orbits. For the circular case, the value $1/3$ was found to be a good choice for numerical purposes.

B. Results for the circular case

We begin analyzing the space of initial conditions in terms of the number of bounces, N_b, when the disk moves on a circular orbit. This case shall provide some basic understanding of the numerical results, in particular by comparing them with the analytical considerations of the primitive periodic orbits described above. Similar results are obtained for other scattering functions which behave monotonically when a periodic orbit is approached.

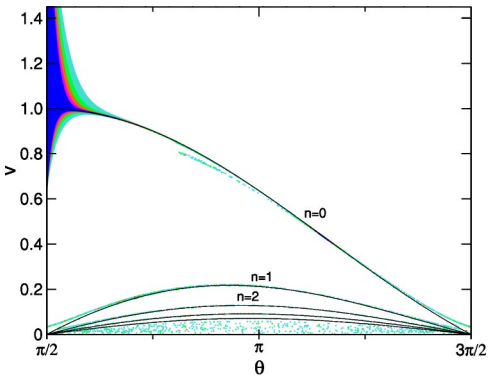

FIG. 2. (Color online) Space of initial conditions for $\varepsilon=0$ ($\alpha=\pi$, $\phi_0=0$). Colors indicate the number of bounces with the disk (from lighter to dark): three bounces (turquoise), four bounces (green), five bounces (orange), six bounces (magenta), and seven and more bounces (blue). The solid curves correspond to the analytical results given by Eq. (5).

Figure 2 shows the space of initial conditions in terms of the number of collisions and the analytical results given by Eq. (5). As expected, the numerical results display a systematic approach towards the analytical curves as the number of collisions increases. However, we note that there are regions where this approach is particularly slow, as in the case of the broad region observed around the curve $n=0$ for θ close to $\pi/2$. Furthermore, there are other regions in the space of initial conditions where certain interesting structures appear which have no apparent relation to the primitive periodic orbits. This can be clearly observed below the curve $n=0$; similar results are also obtained for other values of n.

The broad structure found for $\theta\to\pi/2$ can be easily understood. As observed in [12], the case $n=0$ for the primitive periodic orbits is particular when $\theta\to\pi/2(\beta\to\pi/2)$: The periodic orbit involved is marginally stable, runs following the motion of the disk (direct motion), and its shape approaches the inner circle described by the disk. Clearly, the periodic orbit in question is a whispering-gallery orbit. The marginal stability of these orbits causes the numerical results to converge slowly. Numerical inspection of scattering events in this region confirms this.

Next, we consider the appearance of the snail-like structure in the space of initial conditions (see also Fig. 4 below and [7]). We emphasize that this structure cannot be associated directly to any primitive periodic orbit—i.e., to the consecutive radial collision orbits, since these fulfill Eq. (5). Numerical experiments reported in [7] showed that these structures are related to events where the particle, after a certain number of collisions, loses almost all its kinetic energy. The outcome of this event is extremely sensitive to the initial conditions. A detailed description of the scattering dynamics is presented in Sec. IV.

C. Results for the elliptic orbit

In Fig. 3 we present the space of initial conditions for several values of the eccentricity. We observe first that the overall structure of the charts of the space of initial condi-

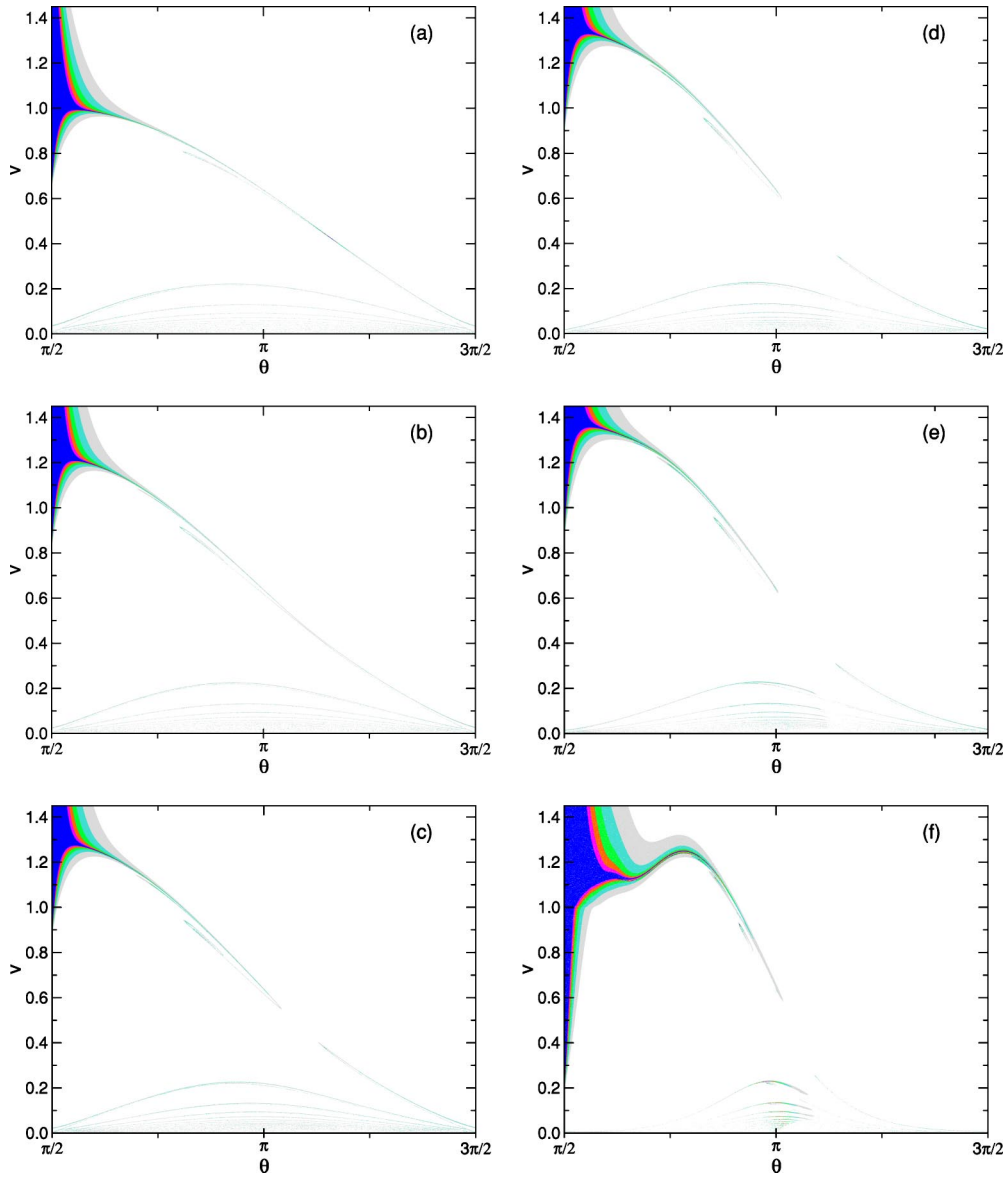

FIG. 3. (Color online) Space of initial conditions for different values of the eccentricity: (a) $\varepsilon=0.001$, (b) $\varepsilon=0.3$, (c) $\varepsilon=0.4$, (d) $\varepsilon=0.5$, (e) $\varepsilon=0.6$, and (f) $\varepsilon=0.8$. Colors indicate the number of bounces with the disk (from lighter to dark): three bounces (gray), four bounces (turquoise), five bounces (green), six bounces (orange), seven bounces (magenta), and eight and more bounces (blue).

tions is essentially maintained for small eccentricities at least up to $\varepsilon=0.3$ and beyond 0.4 up to 0.8 for $n\geqslant 1$. In particular, we note that the n hierarchy (or n curves) of the arrangement of periodic orbits for the circular case is preserved at least for moderate values of the eccentricity. This feature is nontrivial, especially for intermediate or large eccentricities, since the simple geometrical arguments used to obtain Eq. (5) heavily rely on the circular character of the orbit and are not useful for the case of nonvanishing ε. This statement is a consequence of the fact that in the eccentric case the outcome of the collision depends on the value of ϕ where the collision takes place along the orbit of the disk. In the Appendix we present a proof of the existence of periodic orbits for small nonvanishing eccentricities. We note that in this case this proof does explain the hierarchical organization of the periodic orbits in the initial conditions space—i.e., the n-curve

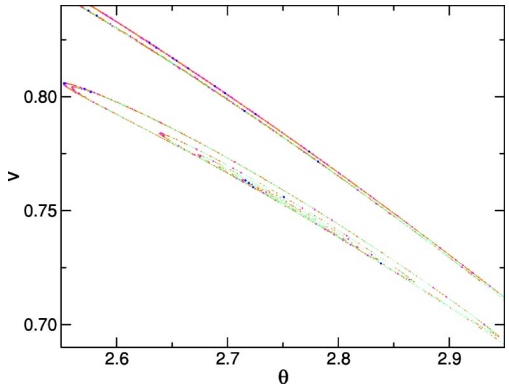

FIG. 4. (Color online) Enlargement of a region of Fig. 3(a) ($\varepsilon=0.001$) illustrating the snail structure (same color code as in Fig. 3).

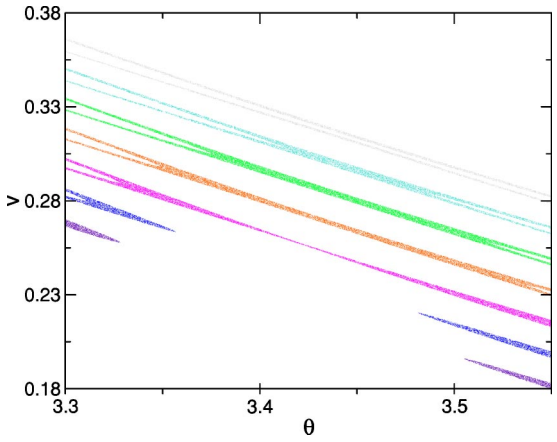

FIG. 5. (Color online) Space of initial conditions for different values of the eccentricity illustrating the bifurcation of the $n=0$ curve (from lighter to darker): $\varepsilon=0.31$ (gray), $\varepsilon=0.32$ (turquoise), $\varepsilon=0.33$ (orange), $\varepsilon=0.34$ (green), $\varepsilon=0.35$ (magenta), $\varepsilon=0.36$ (blue), and $\varepsilon=0.37$ (violet).

hierarchical structure. The dependence upon n appears implicitly in v_0.

We observe that the $n=0$ curves tend to increase the value of v as $\theta \to \pi/2$. This is a consequence of the increase in the velocity at periapsis passage, which follows from angular momentum conservation of the Kepler motion. It is also interesting to note that the snail-like structures encountered previously for the circular case show up again. Figure 4 shows an enlargement of the case $\varepsilon=0.001$ illustrating the snail structure. We observe that the snail structure seems to appear not as an isolated one, but with some companions. This can be noticed in Figs. 3 especially for intermediate and large values of ε, as the stretched region that appears in between the main branch of the $n=0$ structure and the snail structure. In Sec. IV we shall show that the snail structures are related to projections of the homoclinic intersections in the space of initial conditions.

The space of initial conditions that correspond to the two eccentricity intervals mentioned above differ in particular in the behavior of the $n=0$ curve. On the one hand, for values corresponding to $\varepsilon \geqslant 0.4$ the $n=0$ curve is broken into two disjoint segments which fold back and therefore are not individually defined for the whole range of θ. Thus there exist events which display many bounces with the disk, related to the $n=0$ orbit, but not for all values of θ. On the other hand, for $\varepsilon \leqslant 0.3$ the two manifolds appear to be connected and are defined in the whole range of θ. This clearly points out to the occurrence of a bifurcation which may create or destroy periodic orbits by varying ε. Details of this bifurcation are shown in Fig. 5. The two initially separated stable manifolds approach each other systematically. For eccentricities around $\varepsilon \sim 0.33$ $(0.32 \leqslant \varepsilon \leqslant 0.35)$ the manifolds seemingly merge, and beyond 0.35 they separate again folding back. The exact value of ε where the bifurcation takes place depends on the value ϕ_0 considered to sample the space of initial conditions. While the charts of initial conditions provide no further information about this bifurcation, they clearly exhibit regions in the space of initial conditions where interesting behavior may show up. We mention that this type of bifurcation also occurs involving other n curves in the space of initial conditions. These cases are more difficult to study numerically, due to the accumulation of the n curves towards zero [cf. Eq. (5)].

For $\varepsilon=0$ the stable manifolds of the n curves also merge, in general into two distinct positions. This follows from the fact in the circular case there exist regions in the parameter space where the radial collision orbits are stable. In this case, the development of the horseshoe construction is such that the new periodic orbits are created through saddle-center bifurcations by changing the Jacobi integral. This occurs when the invariant manifolds intersect at the symmetry line. We therefore expect that interesting scattering behavior occurs for small values of the eccentricity, relatively close to the position on the space of initial conditions, where such saddle-center bifurcations take place. Indeed, as we shall show in the next section for a particular value of ε (which is far from the bifurcation illustrated in Fig. 5), the scattering functions display a large number of collisions. This is necessary, though not sufficient, for the existence of regions in phase space where the motion is bounded.

Other interesting features also apparent in the charts of initial conditions (Fig. 3) are related to the effective shrinking of the "trapping region" as the eccentricity of the Kepler orbit is increased. In particular, we mention the value $\varepsilon_1=1-d/a$, where the disk covers the foci at the turning points, thus inducing changes in the local properties (curvature) at the turning points, and the value $\varepsilon_2^2=1-(d/a)^2$, where the trapping region shrinks to a point.

IV. STRUCTURE OF THE SCATTERING FUNCTIONS FOR $\varepsilon=0.001$

In this section, we shall study specific scattering functions for the case $\varepsilon=0.001$. The main motivation to consider such small yet nonzero eccentricity comes from the data corresponding to the shepherd satellites of Uranus and Saturn. The scattering functions will be functions of one variable, the initial magnitude of the outgoing velocity v, which follows after fixing the value of the angle θ. The latter will be specified using the results of the initial conditions space, in such a way that by changing v there is an intersection with the regions that display many collisions with the disk (cf. Fig. 3). In particular, we shall consider the number of bounces N_b and/or the escape time T_e, which is the time that the particle requires to leave the scattering region. These quantities are related to each other in general, and thus some information is redundant. Yet for the study of the snail structure together they provide a clear picture of the scattering dynamics as we shall see below.

We shall study two regions of the initial conditions subspace: First, we address the question of the existence of trapped motion for nonzero eccentricity. We present results on a region where the corresponding $n=0$ curve in the circular case displays stable radial-collision periodic orbits (retrograde motion). Second, we consider the dynamics around the snail structure displayed in Fig. 4.

A. Trapped motion

The structure of the initial condition space for small values of the eccentricity resembles closely that of the circular

case, displaying the n curves hierarchical arrangement and the snail structures. It is thus natural to expect that the scattering dynamics of this case mimics those of the circular case. In particular, we are interested in the question of the existence of regions in phase space of purely trapped motion—that is, regions where the particle is trapped dynamically through consecutive collisions with the disk. These regions are of interest in connection with the occurrence of narrow rings in the presence of shepherd moons [12–15]. We emphasize that the existence of these regions of trapped motion is not a trivial extension of what happens in the circular case, for at least two reasons. First, for nonvanishing ε there is a complicate dependence of the collision output on the disk's orbital position ϕ. Second and more important, the argument that leads to prove the existence of stable periodic orbits for the circular case, and hence regions of trapped motion, relies on the generic character of the saddle-center bifurcation. Such argumentation is valid *only* when a single parameter is varied. In the circular case such a parameter is naturally defined by the only constant of motion, the Jacobi integral. In contrast, the lack of this integral of motion in the eccentric case involves thus two-parameter bifurcations.

Inspection of the space of initial conditions shows a large number of collisions in an interval close to $\theta \approx 3.62$. This interval is close to the location where the $n=0$ stable periodic orbits are located. In Fig. 6 we present the number of collisions as a function of the initial velocity v for some values of θ. Similar results are obtained for T_e. Figures 6(a) and 6(d) show the typical structure found in systems displaying fully developed topological chaos. However, comparing the results for different values of θ, we notice that the structure of the scattering functions actually changes. Concretely, for $\theta = 3.55$ in Fig. 6(a), we have the usual two-peak Cantor set structure: At least for the low-lying hierarchical levels, each interval of continuity [18] splits into two in the next level. This is consistent with the dominance of the hyperbolic component of a binary horseshoe, up to the level of development numerically considered. In contrast, in Fig. 6(b) we observe for $\theta = 3.6$ that the neat Cantor structure is now dominated by one of the peaks. Some of the intervals of continuity split into two peaks in the next hierarchical level, while others do not do it until a higher level. Such a structural change in the scattering functions is associated with pruning—i.e., with the appearance of nonhyperbolic components in the chaotic saddle which dominate the scattering dynamics. In addition, the maximum number of bounces is increased and we observe trajectories displaying up to 50 bounces. Similar results displayed in Fig. 6(c) are obtained for $\theta = 3.65$. Finally, for $\theta = 3.7$, the structure of the scattering functions displays again the two-peak Cantor set structure.

Pruning is not sufficient to imply trapped motion though. Further inspection of the scattering dynamics for θ between 3.6 and 3.65, as suggested by the structure of the scattering functions, displays an extremely large number of bounces. In Fig. 7(a) we have plotted the first 100 bounces of a trajectory that displays more than 10 000 collisions. We emphasize that, in a strict sense, this orbit may not be trapped. This is a consequence of the large dimensionality of this system. For nonzero eccentricity the system has two and a half degrees of freedom, and therefore Arnold diffusion may play an important role. However, the time scale for Arnold diffusion to be relevant is (exponentially) large [19], and therefore, for practical purposes we can consider it to be a trapped orbit.

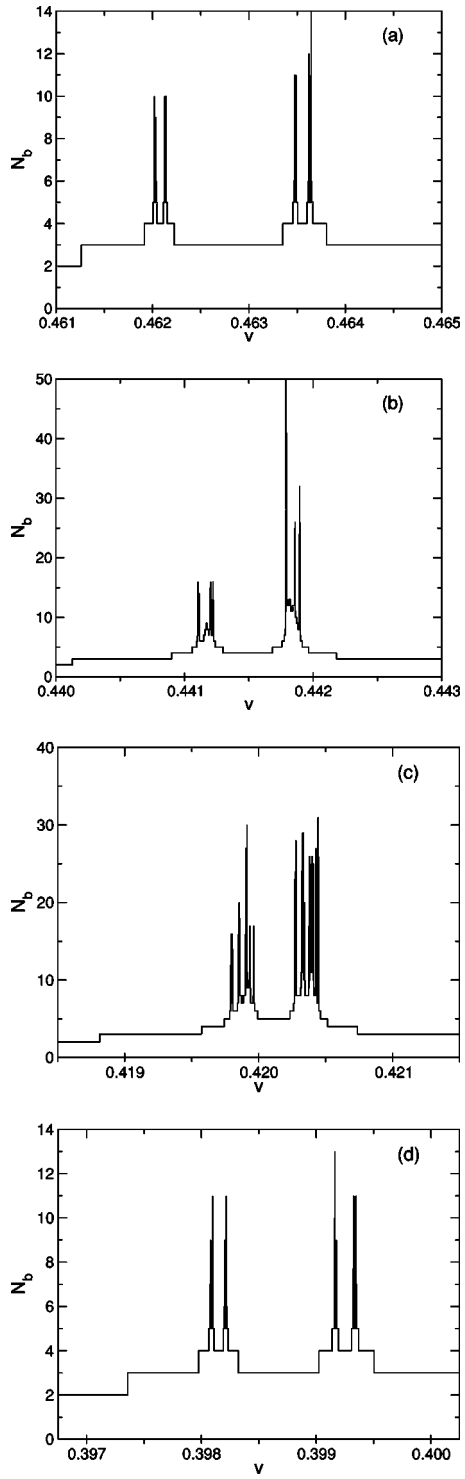

FIG. 6. Number of bounces, N_b, as a function of the initial velocity v for different values of θ. (a) $\theta = 3.55$, (b) $\theta = 3.6$, (c) $\theta = 3.65$, and (d) $\theta = 3.7$. The change in the structure of the scattering functions, which is associated with pruning, suggests the possible existence of trapped orbits.

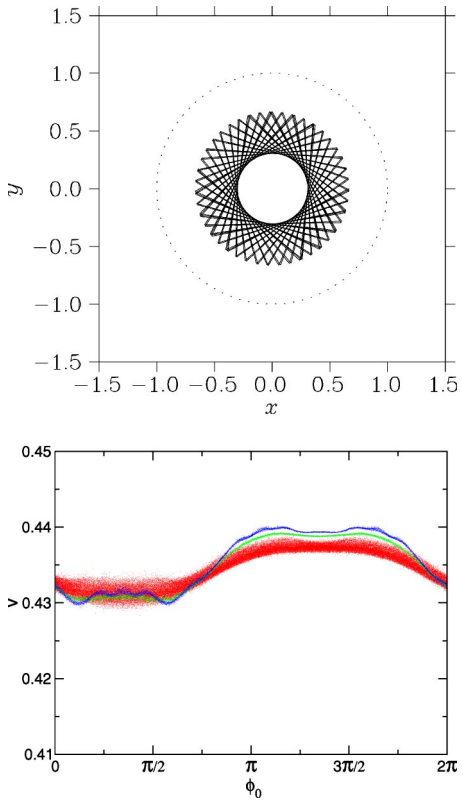

FIG. 7. (a) First 100 bounces of a trajectory displaying at least 10 000 collisions ($\varepsilon=0.001, \theta=3.62, v=0.4332, \ldots$). (b) (Color online) Projection into the ϕ_0 vs v space of the trajectories which bounce at least 1000 times with the disk, characterizing the trapped region for distinct values of the eccentricity: $\varepsilon=0.001$ (red/gray), $\varepsilon=0.0015$ (green/light gray), and $\varepsilon=0.0016$ (blue/dark gray). For comparison, the trapped region of the circular case is distributed uniformly on ϕ_0 in the interval $0.437 \geqslant v \geqslant 0.42$.

Figure 7(b) shows in the projection in the space v vs ϕ_0 of the set of orbits with at least 1000 collisions for several values of ε. For a given eccentricity, Fig. 7(b) provides a qualitative picture of the measure of the trapped orbits associated with the $n=0$ retrograde family. As expected, the measure of this set diminishes for increasing eccentricity. The case of circular motion corresponds to a uniform distribution on ϕ_0 and v located in the interval $0.437 \geqslant v \geqslant 0.42$. We notice that the uniform distribution of the circular case is quite sensitive to breaking the rotational symmetry of circular motion for nonzero ε—i.e., the constancy Jacobi integral. This is nicely illustrated with the rather small values of ε plotted in Fig. 7(b).

Finally, an alternative way to show that trapped motion exists is to use the escape rate. The escape rate of a hyperbolic system shows an exponential behavior in contrast to the nonhyperbolic cases which show an algebraic decay law, with an exponent near to 2 [20]. If one distributes projectiles in the interaction region, one can numerically obtain the exponent of the decay law. If the number of projectiles in the tail of the scattering experiment is *much higher*, in a nonstatistical way, than the one expected by the escape law, it can be concluded that a stable island exists in that interaction region. In Fig. 8 the differential escape rate is shown for ε

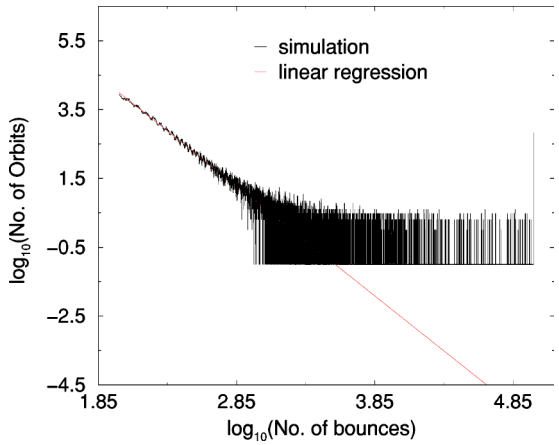

FIG. 8. (Color online): Differential escape rate for initial conditions encircling the trapped region ($\varepsilon=0.001\,65$). The red straight line shows the (initial) algebraic decay expected in this situation. The peak at the right of the plot indicates a large number of particles that do not escape.

$=0.001\,65$. Focusing on the tail, there is a nonstatistical pronounced peak at the cutoff of the number of bounces. This indicates the existence of a stable island for this eccentricity.

B. Scattering dynamics on the snail structure

Now we analyze the relevant aspects of the dynamics for trajectories with initial conditions corresponding to the snail structure displayed in Fig. 4. We recall that the numerical results illustrated in the charts of initial conditions are quite generally interpreted as the intersection of the stable manifolds of some invariant structure in phase space with the hyperplane that defines the chart. This is therefore related either to the unstable periodic orbits, to the existence of other stable periodic orbits or to the existence in phase space of parabolic manifolds or other structures displaying marginal stability. Yet from the charts of initial conditions no stability properties of the scattering events associated with these structures can be inferred. We thus perform further one-parameter scattering experiments.

In Fig. 9 we display the number of collisions, N_b, and the escape time T_e for $\theta=2.74$. We observe the dramatic change in the structure of the number of bounces in comparison to the results displayed in Fig. 6. The scattering functions show characteristic accumulation of peaks. Interestingly, while the number of collisions remains moderate (on the scale displayed), the escape time increases dramatically as we approach the accumulation point. We are led to conclude that the scattering trajectories must display a collision with the disk such that the outgoing velocity is remarkably small. This is consistent with the $1/v$ type of behavior displayed in the escape time. Inspection of individual scattering trajectories confirms this. We shall thus refer to these characteristic peaks as the low-velocity peaks [21]. We mention that this behavior is also observed in the circular case by performing scattering experiments of constant initial energy, which probe different Jacobi integrals [7], and have also been observed in a one-dimensional time-dependent model of par-

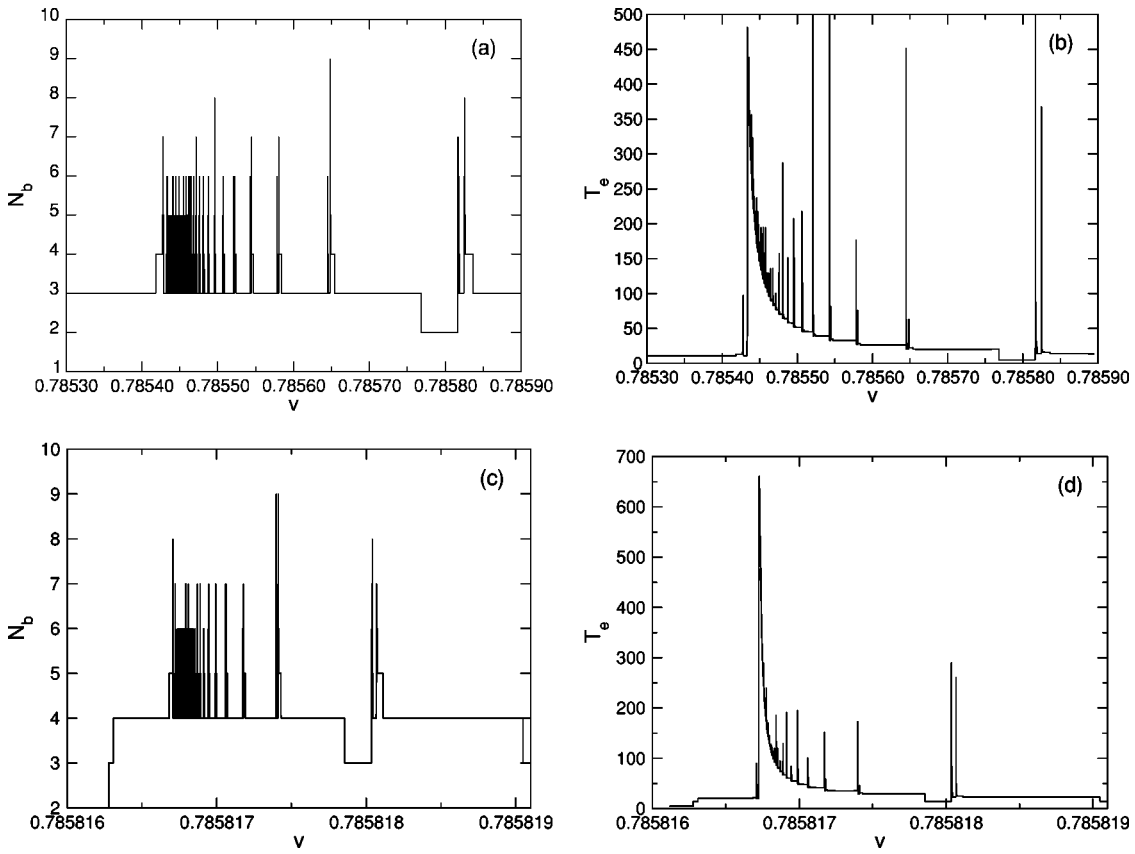

FIG. 9. Structure of the scattering functions (number of collisions, N_b, and escape time T_e) for initial conditions in the snail structure.

ticle transport in an open hydrodynamical flow [22].

Inspection of the scattering functions and individual trajectories reveals that there is some systematic behavior. We notice first that each low-velocity peak is accompanied by a partner. Moreover, the low-velocity peaks display a kind of fractal structure and thus suggest the existence of homoclinic and heteroclinic connections of some invariant structure in phase space. Scattering trajectories corresponding to a certain low-velocity peak lose almost all velocity after the kth collision. Different low-velocity peaks can be classified by the first collision where a significative amount of kinetic energy is lost. Within one such peak, the scattering trajectories of nearby intervals of continuity [18] differ in T_e, to a very good approximation, by a constant quantity. Indeed, the intervals of continuity can be characterized by the number of full turns of the disk between the collisions k and $k+1$—i.e., between the (first) collision where the particle looses most of its energy and the next one. By consequence, this difference in time is very close to 2π, which is the period of the orbit of the disk. We may thus introduce a new label $I_{(k)}$ to classify the corresponding interval of continuity of the scattering trajectory. Second- and higher-order low-velocity peaks are associated with later collisions of this type—i.e., which take away most of the energy of the particle in later collisions. This characterization corresponds to a symbolic description of the dynamics for scattering events on the snail structures, even though the snail structures have not been associated with the simple periodic orbits of the system. Further details and constraints on the application of this symbolic dynamics for the snail structures require further investigation.

Numerical results for $\varepsilon=0$ suggest that the snail structures are related to the projection of the homoclinic and heteroclinic intersections of the manifolds of the radial collision periodic orbits, first, and second, with the overall bifurcation scenario [23]. This is consistent with the fractal behavior mentioned above. After the first development of the horseshoe, which by varying the Jacobi integral makes it completely hyperbolic, the tendrils of the invariant manifolds escape. They eventually fold back and reenter the fundamental rectangle in the horseshoe construction. The entrance with $\alpha=\pi$, projected into the initial condition space, is the outermost part of the snail. For positive J, further reduction yields to the next saddle-center bifurcation and the creation of two new periodic orbits. Their corresponding manifolds repeat the above construction: When they fold back and reenter the fundamental rectangle they do it precisely in the middle of all previous ones. So every new passage through $\alpha=\pi$ is projected precisely on the snail structure and also defines the n hierarchy of the primitive periodic orbits. The loops of the snails should scale as $1/n$, since the saddle-center bifurcation scales like that.

V. SUMMARY AND OUTLOOK

In this paper, we have analyzed the scattering dynamics of a restricted three-body problem in two dimensions, which results in a system with a five-dimensional effective phase space. We have based this analysis on known properties of

the particular case of circular orbits where the Jacobi integral is conserved and only one and a half degrees of freedom are relevant. Taking small symmetry breaking as a point of departure, we were able to identify a two-dimensional subspace of initial conditions, which displays relevant properties of the system, without the usual pains of work in high-dimensional spaces.

Our method allowed us to identify initial conditions for which trapping is likely to happen. While our numerical calculations on individual orbits points towards trapped motion (trajectories displaying more than 10 000 collisions) and the escape-rate behavior shows a nonstatistical peak, the high dimensionality of the system allows for effects like Arnold diffusion. Therefore, permanent trapping may not occur and will certainly be difficult to prove. Yet the time scale in which such effect may be relevant is exponentially long [19].

We have also analyzed another unusual feature of the scattering functions: namely, the low-velocity peaks and the corresponding trajectories, which are not directly related to simple periodic orbits of the system. Interestingly, the structure of the time of escape for the low-velocity peaks gives information on the period of the disk, which is obtained only by using asymptotic data. This may be of relevance in the context of the inverse chaotic scattering problem [18]. We constructed an approximate symbolic dynamics which describes the main features of the scattering events involved in this case. This is important because low-velocity peaks are related to parabolic manifolds [21,22], in the sense that the limiting orbit is marginally (un)stable.

The basic idea involved is the reduction to a space of initial conditions of considerably lower dimensionality. Such a reduction may well be essential for practical purposes, e.g., for numerical modeling or for experimental work, where one certainly does not want to search the interesting phenomena in very-high-dimensional spaces of initial conditions, particularly if some system parameters must also be varied. The benefit of such a procedure is to identify regions where interesting and nontrivial scattering dynamics takes place. Yet this benefit will only be obtained if the reduced space of initial condition is chosen adequately; we achieved this by continuation, slightly breaking a continuous symmetry. We would like to emphasize that the dimensional reduction of subspace is desirable quite generally in higher-dimensional systems and that weak symmetry breaking can provide the physical insight needed in a wide variety of situations. However, this method does not *a priori* provide direct information on trapped motion. Future investigations will be directed to describe the chaotic set itself, in particular, to decide on the existence of truly trapped motion. It is important to notice that the subspace of initial conditions we found displayed interesting structures even for large symmetry breaking, where qualitatively different behavior from the symmetric case occurs. One might think of situations, where different symmetries are possible and could be used to define different subspaces, which display similar or complementary features.

ACKNOWLEDGMENTS

We would like to thank C. Jung for helpful discussions and comments. L.B. thanks J. Laskar for the hospitality during his stay at the IMCCE (Obs. Paris), where part of this work was written. We acknowledge financial and travel support provided by the DGAPA-UNAM Project No. IN-101603 and CONACyT Project No. 43375.

APPENDIX

Here, we provide a proof of the existence of the periodic orbits in the problem of scattering off a disk on a Kepler orbit, adapting the method of analytical continuation [24] for this billiard problem.

Consider that the particle collides with the disk. We describe this collision using the angle ϕ to denote the position of the center of the disk. Relative to ϕ, we denote by θ the angle of the velocity, by α the angular position of the collision on the disk, and by J the Jacobi integral (see Ref. [7] for its definition). We notice that the angles used here correspond to those used along the paper, but are defined relative to the angle ϕ. Given the nth collision, the collision $n+1$, which we assume that takes place, is defined by the map f_ε,

$$\begin{pmatrix} \phi_{n+1} \\ \alpha_{n+1} \\ \theta_{n+1} \\ J_{n+1} \end{pmatrix} = f_\varepsilon \begin{pmatrix} \phi_n \\ \alpha_n \\ \theta_n \\ J_n \end{pmatrix}. \tag{A1}$$

In the circular case, the fixed points of this map correspond to periodic orbits if the angle θ satisfies the relation

$$\theta = \frac{\pi}{2m}(2p + m - 2nm), \tag{A2}$$

where p, m and n are 0,1,2,…. In this case, the periodic orbit is closed after m bounces with the disk, and n denotes the number of full turns of the disk between consecutive bounces. In particular, for the circular case, we have

$$f_0 \begin{pmatrix} \phi_n \\ \pi \\ \theta_n \\ J_n \end{pmatrix} = \begin{pmatrix} \phi_n + \delta\phi \mod (2\pi) \\ \pi \\ \theta_n \\ J_n \end{pmatrix}, \tag{A3}$$

where $\delta\phi = (2n-1)\pi + 2\theta$ is the angle difference in ϕ between two successive bounces.

We want to prove the existence of initial conditions for the eccentric case that are mapped onto themselves after m bounces. This condition is fulfilled if

$$f_\varepsilon^m \begin{pmatrix} \phi \\ \alpha \\ \theta \\ J \end{pmatrix} - \begin{pmatrix} \phi \\ \alpha \\ \theta \\ J \end{pmatrix} = 0. \tag{A4}$$

The idea of the proof is to show that Eq. (A4) can be solved perturbatively in ε close to a periodic orbit of the circular case. Neglecting second-order terms, Eq. (A4) is rewritten as

$$(Df^m - \mathbb{1})\begin{pmatrix} \phi - \phi_0 \\ \alpha - \pi \\ \theta - \theta_0 \\ J - J_0 \end{pmatrix} + \varepsilon \frac{\partial f_\varepsilon^m}{\partial \varepsilon} = 0. \tag{A5}$$

Here, Df^m is the derivative of the map at $\varepsilon = 0$ and $(\partial/\partial\varepsilon) f_\varepsilon^m$ is the derivative of the map with respect to ε, evaluated at $\varepsilon = 0$, $\phi = \phi_0$, $\alpha = \pi$, $\theta = \theta_0$, and $J = J_0$.

Due to the conservation of the Jacobi integral for the circular case, all matrix elements of the last row of $(Df^m - \mathbb{1})$ are equal to zero. In order to fulfill Eq. (A5), this implies that the last row of $(\partial/\partial\varepsilon) f_\varepsilon^m$ must have all matrix elements equal to zero. This is indeed the case, as it can be computed directly (for details, see Ref. [23]). So the system of linear equations is reduced by 1. In addition, for the circular case, the dependence on ϕ is trivial. Then, the system of linear equations has the form

$$\mathbf{B}(m)\begin{pmatrix} \alpha - \pi \\ \theta - \theta_0 \\ J - J_0 \end{pmatrix} = -\varepsilon \frac{\partial \hat{f}_\varepsilon^m}{\partial \varepsilon}. \tag{A6}$$

Here, the matrix $\mathbf{B}(m)$ is given by the matrix $(Df^m - \mathbb{1})$ omitting the first column and the last row, and $\hat{f}_\varepsilon^m$ represents the corresponding map.

In order to have a solution of Eq. (A6), this determinant of the matrix $\mathbf{B}(m)$ must be different from zero. The determinant can be written as

$$\det[\mathbf{B}(m)] = Cm(\lambda^{m/2} - \lambda^{-m/2})^2, \tag{A7}$$

where λ is the eigenvalue corresponding to the fixed point of the circular case and C is a constant independent of m. This expression can only be zero for $\lambda^m = 1$. Alternatively, from the expression for $\mathbf{B}(m)$, we obtain

$$\det[\mathbf{B}(1)] = -\frac{R\delta\phi^3}{d(R-d)^2\cos(\theta_0)^2}. \tag{A8}$$

This expression can only be zero if $\delta\phi$ is zero—i.e., if the angle difference between two successive bounces would be zero. Therefore, in the cases $\delta\phi = 0$ and $\lambda^m = 1$ we cannot continue the periodic orbits of the circular case to the eccentric case. Otherwise, the matrix $\mathbf{B}(m)$ can be inverted and the system of linear equations (A5) has exactly one solution. This establishes that the fixed points of the circular map can be deformed for nonzero ε and yield periodic orbits of the eccentric case.

[1] C. Jung and H. J. Scholz, J. Phys. A **20**, 3607 (1987); **21**, 2301 (1988).
[2] B. Eckhardt, J. Phys. A **20**, 5971 (1987).
[3] P. Gaspard and S. A. Rice, J. Chem. Phys. **90**, 2225 (1989).
[4] Chaos **3**, (4) (1993).
[5] S. Wiggins *et al.*, Phys. Rev. Lett. **86**, 5478 (2001).
[6] T. Uzer *et al.*, Nonlinearity **15**, 957 (2002).
[7] N. Meyer *et al.*, J. Phys. A **28**, 2529 (1995).
[8] G. Gaeta, *Nonlinear Symmetries and Nonlinear Equations* (Kluwer, Dordrecht, 1994).
[9] I. M. Pavlichenkov, Phys. Rep. **226**, 173 (1993).
[10] M. Boiteux, Physica (Amsterdam) **65**, 381 (1973); **75**, 603 (1974).
[11] V. G. Szebehely, *Theory of Orbits: The Restricted Problem of Three Bodies* (Academic Press, New York, 1967).
[12] L. Benet and T. H. Seligman, Phys. Lett. A **273**, 331 (2000); Prog. Theor. Phys. Suppl. **139**, 234 (2000).
[13] L. Benet, Celest. Mech. Dyn. Astron. **81**, 123 (2001).
[14] L. Benet and O. Merlo, Reg. Chao. Dyn. **9**, 373 (2004).
[15] *Planetary Rings*, edited by R. Greenberg and A. Brahic (University of Arizona Press, Tucson, 1984).
[16] A. Morbidelli, *Modern Celestial Mechanics: Aspects of Solar System Dynamics*, Advances in Astronomy and Astrophysics, Vol. 5 (Taylor & Francis, London, 2002).
[17] Z. Kovács and L. Wiesenfeld, Phys. Rev. E **63**, 056207 (2001).
[18] C. Jung, C. Lipp, and T. H. Seligman, Ann. Phys. (N.Y.) **275**, 151 (1999).
[19] V. I. Arnold, Sov. Math. Dokl. **5**, 581 (1964); B. V. Chirikov, Phys. Rep. **52**, 263 (1979).
[20] M. Ding, T. Bountis, and E. Ott, Phys. Lett. A **151**, 395 (1990).
[21] P. K. Papachristou *et al.*, Phys. Lett. A **306**, 116 (2002) P. K. Papachristou *et al.*, Phys. Rev. E **70**, 056215 (2004).
[22] C. Jung, T. Tél, and E. Ziemniak, Chaos **3**, 555 (1993).
[23] O. Merlo, Ph.D. thesis, University of Basel ,2004
[24] C. L. Siegel and J. K. Moser, *Lectures on Celestial Mechanics* (Springer-Verlag, New York, 1971).